Evaluation of Glass Frits for Development of Lead-Free Thick Film Resistor

Xudong Chen[1], W. Kinzy Jones[2]

[1]nScrypt Inc
12151 Research Pkwy Suite 150
Orlando, Florida 32826
xchen@nscryptinc.com

[2]Florida International University,
10555 W Flagler St, EC3442
Miami, Florida 33174
jones@fiu.edu

Abstract

Glass frit is a major component of thick film resistor (TFR) for the production of hybrid circuits. More than thirty commercial lead-free glass frits with different compositions have been evaluated for developing a lead-free thick film resistor that is compatible with typical industry thick film processing and has comparable electrical properties as the lead bearing counterpart. Two glass compositions were selected out of 33 candidates for preparation of RuO_2 based TFR inks, which were screen printed on alumina substrates and fired at 850°C. The preliminary results of these resistors showed that the sheet resistance spanned from 400 ohms per square (Ω/□) to 0.4 mega-ohms per square (MΩ/□) with 5-15% RuO_2 and the hot temperature coefficient of resistance (HTCR) fell in a range of ±350ppm/°C.

Keywords: lead-free, glass frit, thick film resistor, sheet resistance, TCR

1 Introduction

Thick film resistor (TFR) is a composite material in which the conductive phase is embedded in a continuous glass matrix [1]. It has been widely used in hybrid microelectronic circuits [2-5]. Typically the conductive powder (ruthenium oxide, iridium oxide, lead ruthenate) is blended with the glass frit, mixed with an organic vehicle to obtain a printable ink, which is screen printed on an alumina substrate and then fired. Glass frit is one of the major components of a thick film resistor and most of commercially available TFR products contain lead borosilicate glass with significant or even dominant content of lead oxide [6]. To reduce the negative environmental effect due to increasing consumption and disposal of electronic products, lead-free processing has been in high demand. Developing new lead-free thick film materials is one of the most well acknowledged solutions. As a result, there are variety of lead-free solder, conductive and other packaging products available with comparable properties to the lead bearing counterparts; however, only partially satisfactory compositions have been reported for lead-free TFRs. M. Prudenziati et al. [1] prepared RuO_2 based TFRs using seven lead-free glasses. The results, which is inconclusive, evidenced a myriad of complex phenomena, including devitrification, relevant bleeding of the glass on alumina substrates, anomalous distribution of conductive grains in the glassy matrix and phase separation. M. G. Busana et al. [7] used a bismuthate glass and it was claimed that the above negative effects was avoided. However, porous structures were found due to the poor ability of the glass to wet the conductive phase. In addition, the sheet resistance range of these TFRs is limited from ~10Ω/□ to ~1kΩ/□. The work on RuO_2-based lead-free TFRs was not just limited to the reports mentioned above. Many of them remained unpublished and existed as proprietary technical reports to the ink manufacturers.

Glass frit plays a critical role in thick film resistor formulations. It usually occupies 40~98% of the thick film resistor formulation by weight or volume as the primary component and has been considered to contribute significantly to the electrical conduction of TFRs. Glass frit also provides a medium where various types of chemical reactions can occur during the firing process. These reactions greatly contribute to the developed microstructure and hence, to the electrical properties of TFRs. Therefore, it is critical to select a suitable glass material.

In this work, more than thirty commercial lead-free glass frits with different compositions were evaluated, from which the chosen glasses were used for preparation of RuO_2 based TFRs that is compatible with typical industry thick film processing and is able to cover a wide range of sheet resistance with relatively low TCR. In addition to the single glass resistor formulations, a two-glass system was tried to get an intermediary viscosity and wetting so as to contribute properties of each glass to the resistor system.

2 Experiment

2.1 Glass frit evaluation and selection

Each glass powder (from G1 to G33) was pressed into a pill on top of an alumina substrate and fired at 850°C for 10 minutes. Figure 1 shows the firing profile. Although the thickness of a typical TFR film is in the scale of micrometers, the shape and morphology of the fired glass pill in macro scale is indicative of the glass behavior during firing in the application scale. The fired glass pills that demonstrated no cracks and voids, good wetting and bonding to alumina substrate were selected and then evaluated by X-ray diffraction for detection of devitrefication. Thermal analysis including DSC and TGA were also conducted to these pre-selected glasses. Eventually the glasses that meet most of the desired properties were selected for characterization and formulation into resistor inks. A mixture of the selected glasses in a proper ratio was also studied.

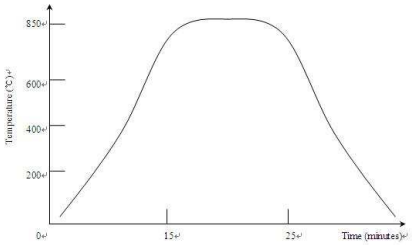

Figure 1 Firing profile for glass and resistor

2.2 Powders and thick film formulation

The selected glasses and original RuO_2 powder were characterized by X-ray diffraction and observed in scanning electronic microscopy (SEM) with energy dispersive X-ray spectrum (EDS).

The inorganic powders were thoroughly mixed by an 18-hour ball-milling process first. Resistor formulations were prepared by mixing different ratios of RuO_2 (5, 10 and 15% by weight) to each selected glass frit and their mixture, and standard organic vehicle (a solution of ethyl cellulose in terpineol). The mixtures were processed on a three-roll mill to yield a printable paste with the desired grind gauge and viscosity. The screen printing process was conducted on a MPM TF-100 micro-printing system with a 325 mesh screen. The printing pattern for resistor electrical property testing is shown schematically in Figure 2. The substrate is 96% alumina. The silver conductor used in this work was C4740S from Heraeus Inc, Conshohocken, PA.

The prepared resistor films were dried at 150°C for 15 minutes and fired at 850°C for 10 minutes using a programmable Lindburg Blue box furnace. The firing profile is the same as shown in Figure 1. The resistance measurement was conducted by a two-probe method on a HP 34401A multimeter at 25°C and 125°C, the hot temperature coefficient of resistance (HTCR) was calculated by:

$$\text{HTCR(ppm/°C)}=\frac{R_{125}-R_{25}}{R_{25}(125-25)}\times 10^6$$

2.3 Material interaction in resistor inks

The inks were evaluated and characterized for microstructure development and materials interactions using X-ray diffraction and SEM with EDS.

X-ray diffraction is considered primary method to evaluate materials interactions. However, polycrystalline alumina as the substrate has a large number of diffraction lines, with a number of peaks that are identical to the major lines of RuO_2, making analysis of RuO_2 on polycrystalline alumina almost impossible. By using a single crystal sapphire (Al_2O_3) substrate cut on the (0001) plane, the only diffraction pattern is from (0006) plane while still providing nearly the same substrate interaction. Figures 3 and 4 shows the diffraction pattern of alumina and sapphire substrate respectively. For comparison, the RuO_2 pattern is also superimposed in the graph. Obviously the diffraction pattern of alumina substrate has multiple peaks and some of them are at same position as RuO_2 peaks. However, single crystal sapphire only has one major peak while the same composition is maintained; therefore it is easier for analysis.

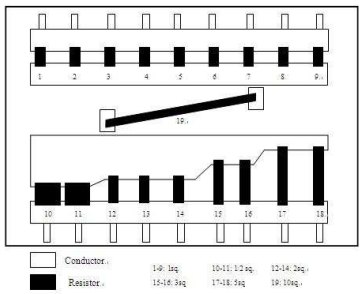

Figure 2 Test pattern for resistor inks

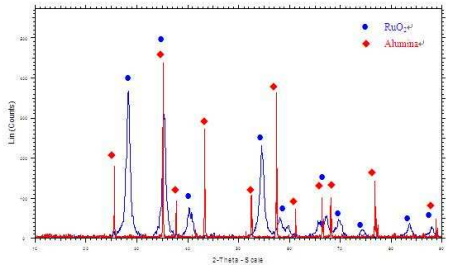

Figure 3 XRD pattern of alumina and RuO_2

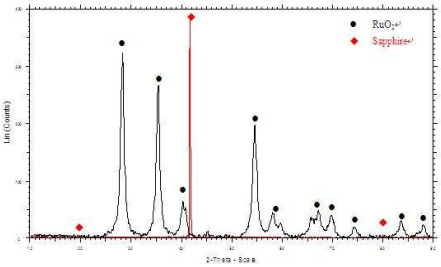

Figure 4 XRD pattern of sapphire and RuO_2

2.4 Analytical methods

The X-ray spectra were collected from the angular region of 10-90° in the 2θ-step scanning mode on a Siemens D5000 diffractometer (Cu Kα radiation, λ=1.544Å). The conditions used were: filament current 40mA, 40kV and step size of 0.01°.

The DSC/TGA was performed on a TA instrument SDT600. The test conditions of were: heating from 50 to 850°C with a ramp rate of 20°C per minute, isothermal hold for 10 minutes at 850°C. The furnace was purged by argon with a 100ml per minute flow rate and air cooled after the experiment.

The SEM and elemental analysis (EDS) were performed with a JEOL JSE-6330F field emission scanning electron microscope. The energy of the electron beam impinging on the sample was 15keV.

3 Result and Discussion

3.1 Glass selection and characterization

Typically, the glass should possess a proper coefficient of thermal expansion (CTE) to match the CTE of the alumina substrate in order to prevent potential thermal stress that usually results in cracks or inferior interface bonding after fire processing. Good wetting to the substrate is another property to ensure good adhesion to the substrate. A suitable softening point is required for the glass to melt and have proper viscosity so that a desired microstructure of the thick film can be obtained. The major composition may vary somewhat in fraction but typically consists of the oxides of essential elements such as B_2O_3 and SiO_2. Other oxides have various functions such as providing the mechanical strength, lowering the softening point, provide the desired reactions and etc. In this work there is no specific requirement for the glass composition except those containing large fraction of ZnO, which is considered as one of the most reactive ingredients and the major cause of devitrification after firing. Moreover, the electrical properties also depend on the film geometry; therefore the glass should maintain its shape after firing. This requires the glass to be dense and compact after firing.

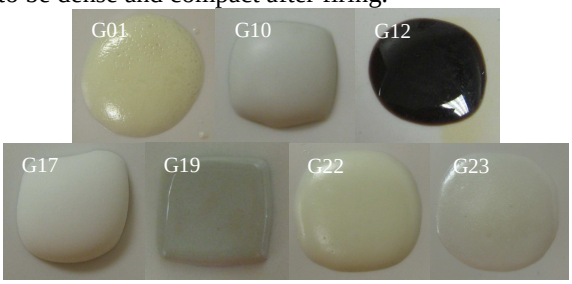

Figure 5 Pre-selected glasses (after firing)

Every glass candidate was evaluated based on the fired pills as well as the basic properties. Figure 5 shows the pictures of the seven glasses (G01, G10, G12, G17, G19, G22 and G23) that meet the property criteria set for the pre-selection as following:

- ✓ Composition: with no large content of ZnO.
- ✓ Softening point (T_s): Between 400°C and 700°C.
- ✓ CTE: Match the CTE of alumina substrate (65-75×10^{-7}/°C), preferably less.
- ✓ Good wetting to the alumina substrate.
- ✓ Dense and compact after firing.
- ✓ No significant expansion and shrinkage.

The fired pills of these seven glasses were further investigated by X-ray diffractometry. Since the X-ray beam can only penetrate tens of microns at most, the scanned area of the fired glass pill can be considered as pure glass. The results showed some broad peaks which are crystallized silica in nano-scale in fired glass samples G01, G10, G17, G22 and G23. The DSC data demonstrated the devitrefication of these glasses as well. Only G12 and G19 remained vitreous after firing. The weight change of all glasses is no more than 2% according to the TGA data. Therefore, G12 and G19 were selected for resistor formulation.

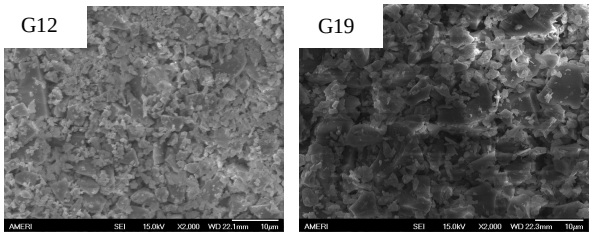

Figure 6 SEM images of glass powder G12 and G19

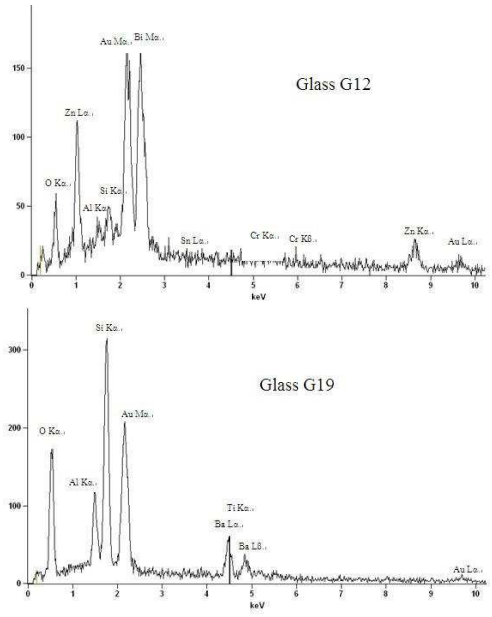

Figure 7 EDS spectrum of glass G12 and G19

Figure 6 shows the SEM micrographs of the glass frits G12 and G19. The average particle size of G12 is around 2μm but large particles (>5μm) exist. The particle size of G19 is a bit larger, some of them even larger than 10μm. Figure 7 shows the EDS spectrum of glass powder G12 and G19 respectively. The gold Mα peak at around 2.1keV and Lα peak at

around 9.7keV are from the coating on the glass powder during SEM sample preparation. Based on the product description of the glass frits and the EDS data, the major composition of glass G12 is B_2O_3-SiO_2-Bi_2O_3-ZnO and there are small fractions of Al, Cr and Sn oxides. The major composition of glass G19 is B_2O_3-SiO_2-BaO-Al_2O_3 with a trace of Ti. The element boron can not be effectively detected using EDS due to its low atomic number.

Figures 8 shows high magnification SEM micrographs of fired G12 and G19. It can be seen that glass G12 completely melted and a relatively uniform microstructure was developed after firing. The small cracks at the white regions might due to over-firing. But the overall structure is dense and compact. There are no major voids and it can be inferred that glass G12 has a lower viscosity during firing. Fired G19 exhibited voids and the high magnification micrograph shows some non-melted glass particles around or in these voids. There might be several reasons for this. First of all, the softening point of G19 is around 780°C and the 850°C peak temperature for 10 minutes firing might not be sufficient to melt the entire glass particles. Secondly, it is normal that some air might be trapped in the melted glass and can not escape due to the large surface tension of melted glass. It can be inferred that this glass has a high viscosity at 850°C.

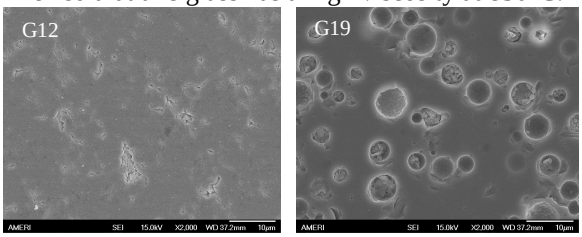

Figure 8 SEM images of fired G12 and G19

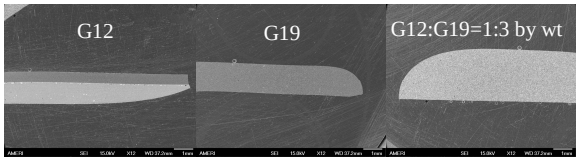

Figure 9 SEM images of fired glass pills cross section

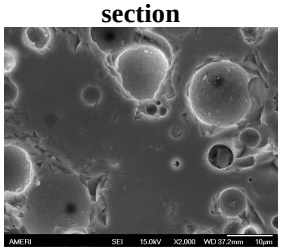

Figure 10 SEM image of fired mixture of G12 and G19 (1:3 by wt)

The viscosity of glass at peak firing temperature and the wetting-ability of glass to the alumina substrate are key factors that determine the film microstructure. Comparing the fired glass pills of G12 and G19, can be seen that G19 might have a higher viscosity than G12 at the firing temperature. By mixing these two glasses in a proper weight ratio, it is expected to obtain an intermediary viscosity and wetting to the substrate. Figure 9 shows the cross section of the fired glass pills of G12, G19 and their mixture (G12:G19=1:3 by weight). It can be seen that the wetting condition of the glass mixture is better than the pure glass G19. Figure 10 shows the microstructure of the fired two-glass mixture. Voids and non-melted glass particles still exist but are less than the pure G19.

3.2 RuO_2

Figure 11 shows the SEM micrograph and EDS spectrum of RuO_2 particles. The actual particles of RuO_2 can not be easily distinguished from the micrograph due to fine particles agglomerate into sub-microns clusters.

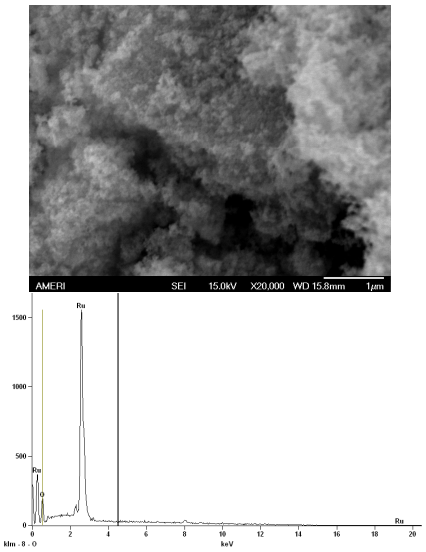

Figure 11 SEM image and EDS of RuO_2 powder

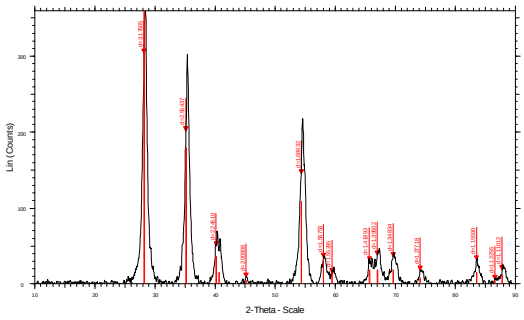

Figure 12 XRD pattern of RuO_2 powder

Figure 12 shows the X-ray diffraction pattern of RuO_2 particles. The spectra were analyzed with DIFFAC Plus EVA Version 10.0 software and the incorporated database. The intensity and position of most peaks match with the standard JCPDS (40-1290) file. From the half width broadening, the diameter D of the RuO_2 grains was computed with the Scherrer formula:

$$D=\frac{k\lambda}{\beta\cos\theta}$$

where k is a constant, typically k=1; β is the corrected line width; θ is the peak position. The average grain size of RuO_2 is around 12 nm based on the calculation.

3.3 Resistor paste

Thick film resistor inks were prepared by mixing different weight ratios of RuO_2 (5, 10 and 15%) to each selected glass frit and their mixture. The inks were evaluated and characterized for microstructure development and materials interactions using X-ray diffraction and SEM with EDS.

3.3.1 Microstructure

Figures 13 to 15 show the SEM micrograph of polished resistor film R12 (refers the resistor ink made from glass G12), R19 (refers the resistor ink made from glass G12) and R12-19 (refers the resistor ink made from glass mixture of G12 and G19) with different RuO_2 fraction. It can be seen that most glass particles melted after firing, which enabled a relatively more uniform microstructure. R19 still has a certain amount of glass particles that were not completely melted, which resulted in a non-fully developed microstructure. Most resistor films exhibited voids and pores. Some researchers [8] compared the number of voids and pores in the same resistor film fired at the same profile in different furnaces. It was evidenced that the films fired in a belt furnace exhibited less voids and pores, appeared more smooth and uniform than the ones fired in a tube furnace. Under the condition of no enough air flow in the box furnace used in this work, the existence of voids and pores is possibly due to the trapped air or gas generated from decomposition of the polymeric materials can not escape from the melted glass with a high viscosity. The spherical shaped voids with a smaller average size raging from 1-2μm appeared in the films are possibly due to reactions occurring between the glass compositions, organic vehicle and RuO_2. Once the temperature reaches to the softening point, inorganic particles start to coalesce towards each other for densification. It is normal that some gas product formed primarily at the interface to diffuse towards the free surface through the dense matrix [9].

The SEM photos also showed that the number of pores and voids increases with increasing glass fraction for most of the films. The possibility that reactions between RuO_2 and the glass composition resulted in voids can be excluded. According to Figures 6 and 8, the fired glass G19 and the glass mixture of G12-19 exhibited quite a number of pores and voids, which are obviously inevitable when they were mixed with RuO_2. Figure 8 shows that the pure glass G12 did not exhibit spherical pores and voids after firing. A few of them were found in resistor film R12, which might resulted from the air or gas generated from decomposition of the polymeric materials during firing.

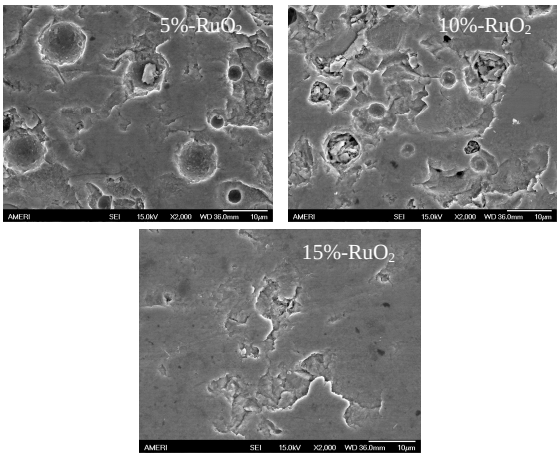

Figure 13 SEM images of R12

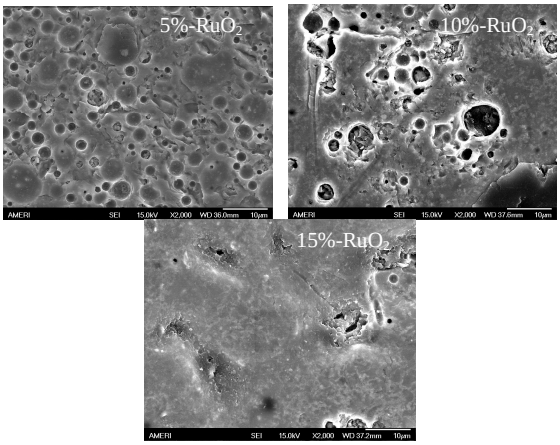

Figure 14 SEM images of R19

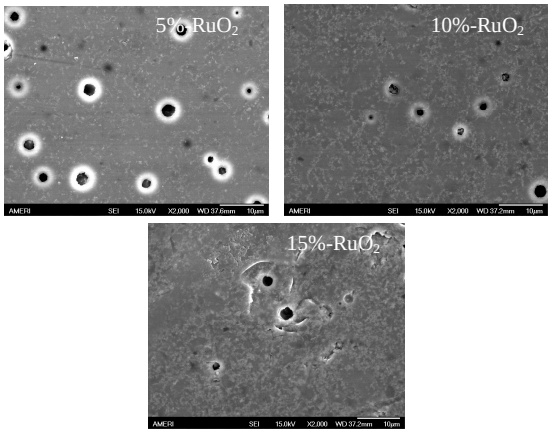

Figure 15 SEM images of R12-19

It can be seen from Figure 13 that the number of pores and voids in the two-glass formulation R12-19 is less than R19. A smoother surface and a relatively uniform microstructure were obtained by mixing glass R12 with glass R19 in a certain ratio (1:3 by weight). Therefore, it is possible to reduce or even eliminate pores and voids by using a glass with better wetting and lower viscosity as an additive to adjust the wetting and viscosity of a glass with high viscosity

and less wetting provided that there is no significant reaction between the two glasses.

3.3.2 Material Interaction

Figure 16 shows the XRD diffraction patterns of resistor film R12 with different RuO_2 fraction. For better comparison, the patterns of sapphire substrate and pure RuO_2 are also superimposed in the graph. The peaks found from the films include two parts. Since the film is only 10 to 20 microns thick, the peaks of single crystal sapphire substrate were still captured at around 20, 37.5, and 80°. The peaks at around 28 and 35° are RuO_2 with a tiny shift comparing to the pure RuO_2 powder diffraction pattern. Several peaks with relatively low intensity between 58 and 65° are also RuO_2. There is no significant difference between the films with different RuO_2 fractions.

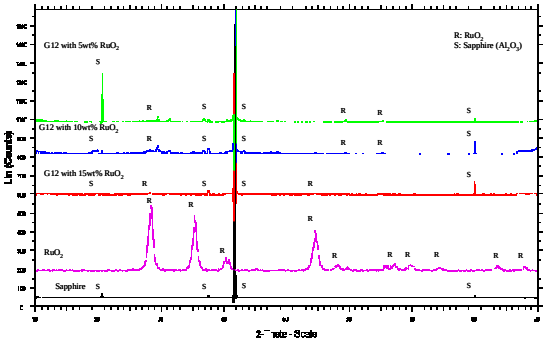

Figure 16 XRD pattern of R12

Figure 17 shows the diffraction patterns of resistor film R19. Almost all peaks came from the sapphire substrate. The relative intensity of the sapphire peaks found in thick films at 20, 37.5, and 80° are much higher than the peaks found from only the substrate. This phenomenon is normal for the cut off axis single crystals. The peaks at 28 and 35° are RuO_2 but the relative intensity is lower than R12. The X-ray diffraction patterns of R12-19 are quite similar to R19 as shown in Figure 18. There was no ZnB_4O_7 [1] and bismuth pyrochlore [7] phase found in the films prepared by these two glasses, which have similar major composition to the ones used in the literature.

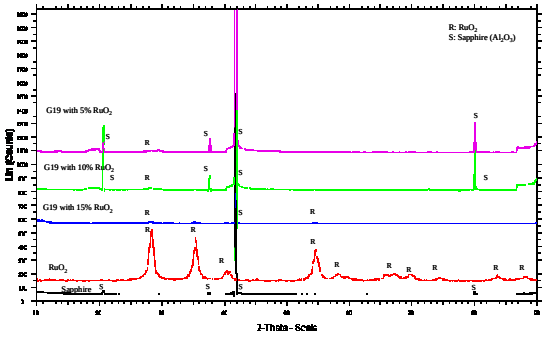

Figure 17 XRD pattern of R19

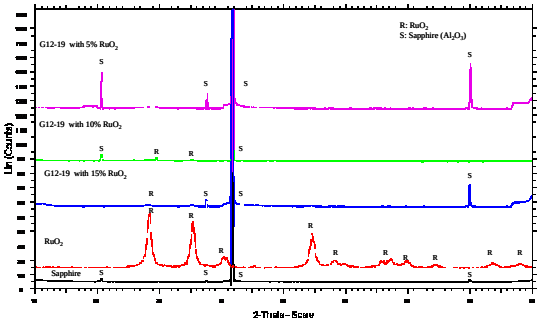

Figure 18 XRD pattern of R12-19

3.4 Electrical property

Figure 19 shows the sheet resistance and TCR result of the obtained three lead-free thick film resistor formulations. Resistor R12 covers a range from several hundred ohms to around 0.4 mega-ohms per square with RuO_2 weight fraction from 15% to 5%. By adjusting the RuO_2 fraction, this formulation has the potential to cover a resistance range (10Ω/□ to 10MΩ/□ in decades) comparable to the lead bearing TFRs. Resistor R19 has a relatively shorter resistance range. The resistance of resistors with 5% RuO_2 is larger than 100MΩ, which is generally considered as an insulator. In addition, according to the raw data, resistor R19 has less repeatability in term of sheet resistance value, probably due to the non-uniform microstructure. Resistor R12-19 has a similar resistance range as R12.

The TCR results showed the typical property of RuO_2 based TFRs, which changes from positive to negative with the increasing of sheet resistance [10]. The negative TCR value indicates a semiconductor-like electrical conduction and the positive TCR indicates a metal-like electrical conduction. Typically, commercial leaded TFRs have a HTCR range of ±50ppm/°C. To obtain a low TCR value, the usual approach to adjust it is to change the chemistry of the ink, namely to include in the ink small amounts of additives. For example, MnO_2, CdO, Rh_2O_3, V_2O_5 are added as negative TCR drivers while conversely Cu and precious metals are used as positive TCR drivers [4]. Generally, type and amount of TCR modifiers as well as the characteristic of conductive and glassy phases are selected on the basis of experience or trail and error approach since no predictive model is available yet. Without any additives, the HTCR of resistors prepared in this work spanned from 250ppm/°C to +350ppm/°C, which can be adjusted to a desired range by adding TCR drivers.

Figure 20 gives the relationship between the sheet resistance and the geometry of the resistors containing 15wt% RuO_2. It is clear that resistor R19 and R12-19 have an inverse size effect [11]. Resistor R12 exhibited a slight size effect [12] comparing to the others. The research on size effect and the interaction between the resistor film and conductor

termination is beyond the scope of this study. Further investigations are required to support these hypotheses.

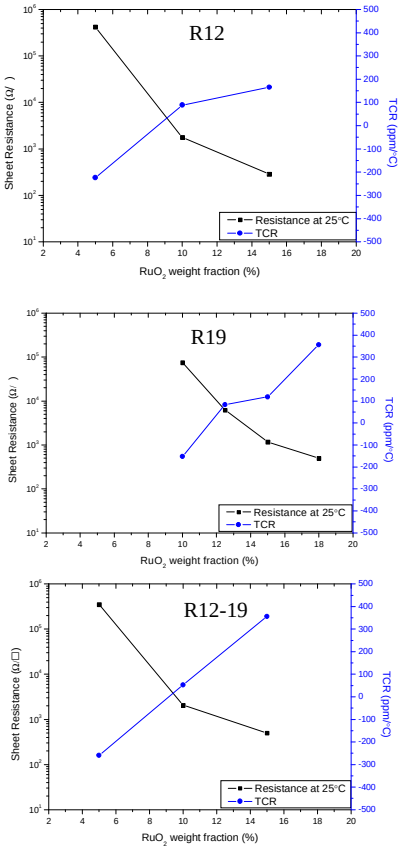

Figure 19- Resistance and TCR of resistor films

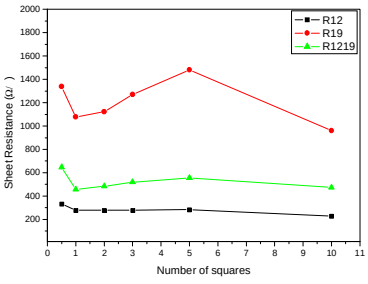

Figure 20- Relationship between number of squares and sheet resistance of resistor with 15% RuO_2

4 Summary and conclusion

A progress in search of suitable glass material to develop a RuO_2-based lead-free thick film resistor has been provided in this work by evaluating thirty three commercially available electronic grade lead-free glass frits. The main achievements of this work are summarized as following:

1. Two lead-free borosilicate glasses R12 (B_2O_3-SiO_2-Bi_2O_3-ZnO) and R19 (B_2O_3-SiO_2-BaO-Al_2O_3) have proper wetting and good bonding to the 96% alumina substrate, and a CTE that matches with the alumina substrate. They are suitable to be fired under the most commonly used industry peak temperature and remain vitreous after firing.

2. Resistors prepared using glass R12 cover a sheet resistance range from 400 Ω/□ to 0.4 MΩ/□ with a variation of RuO_2 weight fraction from 5 to 15%. This formulation has quite a potential to cover a resistance range from 10Ω/□ to 10MΩ/□ by further tuning the RuO_2 fraction.

3. An intermediate wetting to the alumina substrate and variation in the viscosity of the glass material was obtained by mixing two selected glasses in a certain weight ratio (R12:R19=1:3). Resistors prepared using this mixture exhibited a relatively more stable sheet resistances than resistors prepared using only R19. In addition, this two-glass resistor system overcame the phenomenon of glass bleeding onto conductor terminations in the formulation of R12 with low RuO_2 weight fraction (≤5%). The sheet resistance of R12-19 spans from ~500Ω/□ to 0.35MΩ/□ with a variation of RuO_2 weight fraction from 5 to 15%.

4. All of the resistors prepared using each glass and their mixture exhibit relatively low (in the range of -250 to 350ppm/°C) HTCR values without the additions of any TCR drivers.

Generally, the prepared RuO_2-based resistors in this work exhibit superior electrical property than the work reported previously. It can be concluded that a RuO_2 based lead-free thick film resistor that can cover a wide sheet resistance range could be developed by selecting a suitable glass material and well controlled process. It is expected that improvements can be achieved by further work on these RuO_2-based lead-free TFRs. More extensive studies are required to collect data on glass viscosity temperature dependence, resistor film microstructure development and ingredient material interactions, from which a better understanding of reaction kinetics and conduction mechanism of these lead-free TFRs might be obtained.

Reference

[1] M. Prudenziati, F. Zanardi, B. Morten. Lead-free thick film resistors: an explorative investigation. Journal of Materials Science: Materials in Electronics 13 (2002), 31-37.
[2] D. W. Hamer, J. V. Biggers. Thick Film Hybrid Microcircuit Technology. John Wiley & Sons Inc., New York, 1972.
[3] R. W. Vest. Conduction Mechanisms in Thick Film Microelectronics. Ph.D Dissertation, College of Engineering, Purdue University. West Lafayette, 1980.
[4] M. Prudenziati. Thick Film Sensors. Elsevier Science, 1994.
[5] Tapan K. Gupta. Handbook of Thick- and Thin-Film Hybrid Microelectronics. John Wiley & Sons Inc., Hoboken, New Jersey, 2003.

[6] J. Setina, V. Akishin, J. Vaivads. Glass composition for the thick-film resistors. Materials Science Forum, Vol. 502, Dec 2005, 231-236.
[7] M. G. Busana, M. Prudenziati, J. Hormadaly. Microstructure development and electrical properties of RuO_2-based lead-free thick film resistors. Journal of Materials Science: Materials in Electronics, 17 (2006), 951-962.
[8] A. Kshirsagar, S. Rane, U. Mulik, D. Amalnerkar. Microstructure and electrical performance of eco-friendly thick film resistor compositions fired at different firing conditions. Materials Chemistry and Physics, 101 (2007) 492-498.
[9] Wenjea J. Tseng, Chir-JangTsai, Shen-Li Fu. Porosity development of RuO_2 filled glass thick films on aluminum nitride substrates at elevated temperatures. Journal of Materials Science: Materials in Electronics, Vol. 11 (2000), 411-417.
[10] Toshio Inokuma, Yoshiaki Taketa, Miyoshi Haradome. The microstructure of RuO_2 thick film resistors and the influence of glass particle size on their electrical properties. IEEE Transactions on Components, ybrids, and Manufacturing Technology, Vol. CHMT-7, No. 2, June 1984, 166-175.
[11] M. Prudenziati, B. Morton, L. Moro, L. Olumekor, A. Tombesi. Interactions between thick-film resistors and terminations: the role of bismuth. Journal of Physics D: Applied Physics, 19 (1986), 275-282.
[12] M. Prudenziati, F. Sirotti, M. Sacchi, B. Morten, A. Tombesi, T. Akomolafe. Size Effects in Ruthenium-Based Thick-Film Resistors: Rutile VS. Pyrochlore-Based Resistors. Active and Passive Electronic Components, Vol.14 (1991), 163-173.